

Danila F., Quick W., White R., von Caemmerer S., Furbank R.T. Response of plasmodesmata formation in leaves of C₄ grasses to growth irradiance. *Plant Cell Environ.* 2019;42:2482–2494. <https://doi.org/10.1111/pce.13558>, which has been published in final form at <https://doi.org/10.1111/pce.13558>. This article may be used for non-commercial purposes in accordance with Wiley Terms and Conditions for Use of Self-Archived Versions (Publisher journal website as of 11/3/2020)

1 Title

2

3 Response of plasmodesmata formation in leaves of C₄ grasses to growth irradiance

4

5 Authors

6

7 Florence R. Danila^{1,2*}, William Paul Quick^{2,3,5}, Rosemary G. White⁴, Susanne von
8 Caemmerer^{1,2}, Robert T. Furbank^{1,2,4}

9

10 Contact information

11

12 ¹Research School of Biology, Australian National University, Canberra Australian
13 Capital Territory 2601, Australia. ²ARC Centre of Excellence for Translational
14 Photosynthesis, Australian National University, Canberra Australian Capital Territory
15 2601, Australia. ³International Rice Research Institute, Los Baños, Laguna 4030,
16 Philippines. ⁴CSIRO Agriculture and Food, Canberra Australian Capital Territory
17 2601, Australia. ⁵University of Sheffield, Sheffield, United Kingdom.

18

19 *To whom correspondence should be addressed. E-mail:

20 florence.danila@anu.edu.au

21

22 Funding

23

24 This research was funded by the Australian Government through the Australian
25 Research Council Centre of Excellence for Translational Photosynthesis
26 (CE1401000015).

27

28 Abstract

29

30 Rapid metabolite diffusion across the mesophyll (M) and bundle sheath (BS) cell
31 interface in C₄ leaves is a key requirement for C₄ photosynthesis and occurs via
32 plasmodesmata (PD). Here, we investigated how growth irradiance affects PD
33 density between the M and BS cells and between M cells in two C₄ species using our
34 PD quantification method, which combines three-dimensional laser confocal

35 fluorescence microscopy and scanning electron microscopy. The response of leaf
36 anatomy and physiology of the NADP-ME species, *Setaria viridis* and *Zea mays* to
37 growth under different irradiances, low light ($100 \mu\text{mol m}^{-2} \text{s}^{-1}$) and high light (1000
38 $\mu\text{mol m}^{-2} \text{s}^{-1}$), was observed both at seedling (two weeks after germination) and
39 established (seven weeks after germination) growth stages. We found that the effect
40 of growth irradiance on C₄ leaf PD density depended on plant age and species. The
41 high light treatment resulted in two to four-fold greater PD density per unit leaf area
42 than at low light, due to greater area of PD clusters, and to a lesser extent to greater
43 PD size, in plants grown at high light. These results along with our finding that the
44 effect of light on M-BS PD density in these experiments was not tightly linked to
45 photosynthetic capacity suggest a complex mechanism underlying the dynamic
46 response of C₄ leaf PD formation to growth irradiance.

47

48 **Keywords**

49

50 Plasmodesmata density, growth irradiance, *Setaria viridis*, *Zea mays*, plant age,
51 photosynthetic capacity

52

53 **Abbreviations**

54

55 NADP-ME, nicotinamide adenine dinucleotide phosphate-malic enzyme; PCK,
56 phosphoenolpyruvate carboxykinase

57

58 **Acknowledgements**

59

60 We thank the ANU Centre for Advanced Microscopy (CAM), Australian Microscopy
61 and Microanalysis Research Facility (AMMRF), and CSIRO Black Mountain
62 MicroImaging Centre (BMIC) for providing support and technical assistance. This
63 research was funded by the Australian Government through the Australian Research
64 Council Centre of Excellence for Translational Photosynthesis (CE1401000015).
65 F.R.D is also financially supported by the Lee Rice Foundation scholarship through
66 the International Rice Research Institute, Philippines.

67

68

69 **Introduction**

70

71 High photosynthetic efficiency in C₄ plants is attributed to the ability to concentrate
72 carbon dioxide at the site of rubisco (ribulose-1,5-biphosphate
73 carboxylase/oxygenase), consequently diminishing photorespiration (Hatch, 1987).
74 In a C₄ leaf, fixation of atmospheric CO₂ and photosynthetic carbon reduction are
75 spatially separated into two anatomically and biochemically distinct cells (Kranz
76 anatomy); these are the mesophyll (M) and bundle sheath (BS) cells, respectively
77 (Hatch and Osmond, 1976). The CO₂-tight anatomy of BS cells and high affinity of
78 carbonic anhydrase and phosphoenolpyruvate carboxylase (PEPC) to CO₂ and
79 bicarbonate respectively, contribute to the elevation of CO₂ around the active site of
80 Rubisco to levels up to ten fold ambient CO₂ concentrations in the mesophyll
81 (Furbank et al., 1990; Hatch, 1987; von Caemmerer and Furbank, 2003). While the
82 efficiency of the CO₂ concentrating mechanism is reliant on minimising diffusion of
83 CO₂ out of the BS cells, rapid metabolite exchange between M and BS during C₄
84 photosynthesis is required to support photosynthetic flux of C₄ acids to the BS cells
85 and for C₃ products to return to the mesophyll to regenerate PEP. Given that the M-
86 BS cell interface is characterised by cell walls which are heavily thickened and often
87 suberised, metabolites must pass symplastically across this barrier, via diffusion
88 through plasmodesmata (PD) (Hatch and Osmond, 1976).

89

90 PD are cytoplasmic conduits that traverse plant cell walls to enable intercellular
91 continuity. Evidence for the existence of PD in plants was published more than a
92 hundred years ago (Tangl, 1879) but a comprehensive understanding of their role in
93 developmental, intercellular transport and signalling processes as well as their
94 molecular anatomy and genetic networks controlling their function still remains to be
95 realised (Lu et al., 2018). The main challenge underlying PD research has been their
96 minute size and difficulty in viable isolation. For a long time, transmission electron
97 microscopy-based methods have been used to quantify the intercellular PD
98 connections between plant cells using arduous serial sectioning and visual counting
99 of PD (Botha, 1992; Gunning, 1978; Seagull, 1983). This has limited both data
100 accuracy due to the 3-D nature of cell interfaces and patchy, non-random distribution
101 of PD at those interfaces, and statistical robustness due to insufficient sampling
102 coverage. The application of 3-D imaging of intact plant tissue to this problem

103 (Danila et al., 2016) has avoided many of these limitations and provided not only
104 more accurate PD density measurements in leaves but also the first comprehensive
105 PD density survey in monocot species (Danila et al., 2018). In the latter study, C₄
106 grasses were found to have up to 12 times more PD connecting photosynthetic cells
107 compared to the C₃ species (Danila et al., 2018).

108

109 The CO₂ concentrating mechanism of C₄ photosynthesis requires at least 2
110 additional ATP per CO₂ fixed compared to C₃ photosynthesis (Furbank et al., 1990)
111 thus, C₄ plants suffer an energetic penalty under some environmental conditions.
112 Indeed, in natural ecosystems C₄ plants are typically found in high light environments
113 under higher ambient temperatures where the benefits of the CO₂ concentrating
114 mechanism outweigh the costs (Sage and Pearcy, 2000). Nevertheless, in most field
115 situations where C₄ crops and grasses form thick canopies, a substantial proportion
116 of the vegetative part of the plant may experience shade or natural low light. Under
117 such unfavourable conditions, C₄ leaves can undergo both biochemical and
118 anatomical changes as part of their acclimation response (Pengelly et al., 2010;
119 Sonawane et al., 2018; Tazoe et al., 2006). Responses of C₄ plants, however,
120 appear to differ depending on the decarboxylation subtype (NADP-ME, NAD-ME, or
121 PCK), whether the plants are monocots or dicots, or even between species (Tazoe
122 et al., 2006). Photosynthetic efficiency may also be compromised in low light-grown
123 C₄ plants which have been reported to show lower CO₂ assimilation rates compared
124 to high light-grown plants (Sharwood et al., 2014; Sonawane et al., 2018).

125

126 Despite the importance of PD in facilitating transport between M and BS in C₄ plants,
127 there is only one report of the effects of different growth irradiance on PD density in
128 C₄ grass leaves (Sowiński et al., 2007). This study concluded that there was a
129 proportional increase in M-BS PD density with increasing light intensity across all
130 subtypes. However, the transmission electron microscopy technique described
131 above was used, giving a restricted view of PD distribution over this 3D cell-cell
132 interface, hence it is not clear how these changes were achieved. In most tissues,
133 including leaves, PD occur in clusters, one unit of which is termed a pit field.
134 Therefore, the use of the Gunning constant (Gunning, 1978) to calculate PD density
135 in leaves (which requires random distribution of PD on the cell interface, not

136 clustering in pit fields) may not be appropriate for these calculations when PD are so
137 highly clustered in pit fields (Sowinski et al 2007).

138

139 In this study, two NADP-ME C₄ grasses, *Setaria viridis* and *Zea mays*, were grown
140 under different light intensities: low light (100 $\mu\text{mol m}^{-2} \text{s}^{-1}$) and high light (1000 μmol
141 $\text{m}^{-2} \text{s}^{-1}$). The use of *Z. mays* allows comparison with previous studies while the
142 information generated for *S. viridis* adds to the existing knowledge about this new C₄
143 model species with a relatively small sequenced and publicly available genome
144 (Brutnell et al., 2010; Li and Brutnell, 2011). The response of PD frequency between
145 leaf cells to growth under the two different light environments was evaluated by
146 quantifying the PD density between M and BS on the youngest fully expanded leaf at
147 two time points in plant development: two weeks and seven weeks after germination.
148 Implementation of our PD quantification method (Danila et al., 2016) provided detail
149 on how PD density changed expressed both in terms of PD frequency and pit field
150 area. Concurrent with anatomical measurements, the response of photosynthetic
151 assimilation to light intensity was measured and a range of other leaf physiological
152 and anatomical parameters were characterised.

153

154 **Materials and methods**

155

156 **Plant material and growth conditions**

157

158 Seeds of *Setaria viridis* cultivar A10 and *Zea mays* cultivar B73 were germinated in a
159 growth cabinet (High Resolution Plant Phenomics Centre, CSIRO Black Mountain,
160 Canberra, Australia) under two light conditions, 100 $\mu\text{mol m}^{-2} \text{s}^{-1}$ (low light) and 1000
161 $\mu\text{mol m}^{-2} \text{s}^{-1}$ (high light). Cabinets were maintained at 28°C day/22°C night
162 temperatures, 60% relative humidity, 16-hour light/8-hour dark, and ambient CO₂
163 concentration. Plants were supplied with Osmocote (Scotts Australia) and watered
164 regularly. Physiological and anatomical parameters were measured on the youngest
165 fully expanded leaf at two developmental stages: two weeks and seven weeks after
166 germination.

167

168 **Physiological measurements**

169

170 Gas exchange was measured using a LI-6400 equipped with a blue-red light-emitting
171 diode (LED) light source (LI-COR, Inc., Australia) applied to the middle portion of the
172 youngest fully expanded leaf from three independent plants per species. Leaves
173 were initially equilibrated for 30 minutes in a standard environment of 380 $\mu\text{mol mol}^{-1}$
174 CO_2 set in sample cell, 25°C leaf temperature, flow rate of 500 $\mu\text{mol s}^{-1}$, and an
175 irradiance of 2000 $\mu\text{mol m}^{-2} \text{s}^{-1}$. Light response curves were generated by imposing a
176 stepwise decrease in irradiance (2000, 1500, 1000, 800, 600, 400, 200, 100, 0 μmol
177 $\text{m}^{-2} \text{s}^{-1}$), each step lasting for 5 minutes while maintaining temperature and CO_2
178 conditions. Immediately following gas exchange measurements, two sets of 0.6 cm^2
179 leaf discs were collected from the same leaf, one set was snap-frozen in liquid
180 nitrogen and the other set was oven-dried at 60°C for 48 h. Chlorophyll was
181 extracted from the frozen leaf discs using 80% acetone in mortar and pestle.
182 Chlorophyll *a* and *b* proportions of the extract were calculated according to (Porra et
183 al., 1989) using values obtained from Cary® 50 Bio UV-Visible Spectrophotometer
184 (Varian, Inc.) at 663.6, 646.6, and 750 nm wavelengths. Using dried leaf discs, leaf
185 mass per area was obtained by dividing dry weight by leaf area while total leaf
186 nitrogen content was determined on the ground leaf tissue using a CN analyser
187 (LECO TruSpec; LECO Corp., MI, USA).

188

189 **Anatomical measurements**

190

191 All leaf tissue preparations for light microscopy, transmission electron microscopy
192 (TEM), scanning electron microscopy (SEM), and 3-D immunolocalisation confocal
193 microscopy were as described by (Danila et al., 2016). Tissues were collected from
194 the middle portion of the same leaf used for physiological measurement. Leaf tissues
195 were fixed and processed accordingly. For 3-D immunolocalisation confocal
196 microscopy, leaf tissue was fixed and cleared according to (Danila et al., 2016),
197 hybridised with β -1,3-glucan (callose) antibody, followed by Alexa488-tagged
198 secondary antibody, and post-stained with calcofluor white to visualise cell walls
199 (Danila et al., 2016). Transverse sections of resin embedded leaves were imaged for
200 light microscopy under 10X and 40X objectives using a Nikon Eclipse 50i upright
201 microscope (Nikon Instruments). For TEM, ultrathin sections were examined using a
202 Hitachi HA7100 transmission electron microscope (Hitachi High Technologies

203 America) at 75 kV. SEM was performed using a Zeiss Ultra Plus field emission
204 scanning electron microscope at 3 kV.

205

206 To quantify pit field distribution, z-stacks from two leaf tissues per plant were
207 obtained using a Leica SP8 multiphoton confocal microscope (Leica Microsystems).
208 PD density was quantified using the method described in (Danila et al., 2016). PD
209 area and pit field area were measured using SEM images. M-BS PD area per leaf
210 area was calculated according to (Danila et al., 2018). Vein circumference,
211 interveinal distance, and leaf thickness of 10 to 20 individual minor veins were
212 measured from light micrographs of transverse leaf sections. Values for M and BS
213 cell wall thickness, M and BS chloroplast size, M and BS starch granule per
214 chloroplast, M and BS starch granule size, M grana width, and BS chloroplast
215 content were obtained from TEM measurements of transverse leaf sections. Average
216 number of corresponding structures measured was specified in Tables 2 and 3.
217 Because chloroplasts and starch granules were not circular, the measurements
218 performed here were used only for approximate comparison given that all samples
219 were treated the same way. BS chloroplast content was calculated as the proportion
220 of BS cell area taken up by the chloroplasts. BS surface area per unit leaf area (S_b)
221 ($n=7$ or more) was calculated using the equation described previously (Pengelly et
222 al., 2010). A Wacom Cintiq graphics tablet (Wacom Technology Corporation,
223 Vancouver, WA, USA) together with ImageJ software (National Institutes of Health,
224 Bethesda, MD, USA) were used for all anatomical measurements.

225

226 **Statistical analysis**

227

228 Group sizes were equal overall for all response variables. The relationship between
229 various response variables and the main effect (growth irradiance and plant age) and
230 their interactions were obtained using two-way ANOVA (OriginPro 9.1, OriginLab
231 Corporation). Means comparisons were performed using post-hoc Tukey test at 0.05
232 significance level.

233

234 **Results**

235

236 **CO₂ assimilation rate and leaf chemistry**

237

238 In *S. viridis*, light response curves of CO₂ assimilation showed that plants grown
239 under low light conditions had reduced photosynthetic performance when compared
240 to their high light-grown counterparts regardless of plant age (Fig. 1A; Table 1).

241 Similarly, low light-grown *Z. mays* had lower CO₂ assimilation rates than high light-
242 grown plants but there was a significant plant age and growth irradiance x plant age
243 effect on CO₂ assimilation rate (Fig. 1B; Table 1). Low CO₂ assimilation rate in low
244 light-grown plants was particularly evident when plants were measured at high
245 irradiance (Fig. 1C, D). In both *S. viridis* and *Z. mays*, plants grown at low irradiance
246 had 30-50% less leaf mass per area compared to high light-grown plants and across
247 development, high light-grown plants showed a greater leaf mass per area increase
248 over time (Figs. 2A, 3A; Table 1). Significant effect of growth irradiance was also
249 reflected in both total leaf N content (Figs. 2B, 3B; Table 1) and chlorophyll content
250 per leaf area (Figs. 2C, 3C; Table 1) of *S. viridis* and *Z. mays*, where low light-grown
251 plants had lower values.

252

253 **Leaf anatomy**

254

255 There was a significant plant age and growth irradiance x plant age effect on BS
256 chloroplast content and chloroplast size in *S. viridis* (Fig. 2D; Tables 1, 2).
257 Specifically, seven week-old *S. viridis* grown under low light had lower BS
258 chloroplast content (Fig. 2D) but bigger chloroplasts (Table 2) compared to the high
259 light-grown plants. In *Z. mays*, growth irradiance had a significant effect on both BS
260 chloroplast content and chloroplast size (Table 1) where low light-grown plants have
261 lower BS chloroplast content (Fig. 3D; Table 1) and smaller chloroplasts (Tables 1,
262 3) than the high light-grown plants. For both species, smaller leaf veins (Figs. 2E,
263 3E; Table 1), shorter interveinal distance (Figs. 2F, 3F; Table 1), and thinner leaves
264 (Figs. 2G, 4A-D, 3G, 5A-D; Table 1) were observed in plants grown under low light
265 indicative of reduced investment in photosynthetic machinery per unit leaf area,
266 which is also seen in the strong correlation between photosynthetic rate and leaf N
267 content (Supplementary Fig. 1). Transmission electron micrographs also revealed
268 thinner cell walls in both BS (Figs. 2H, 3H; Table 1) and M (Figs. 2I, 3I; Table 1) cells
269 in low light plants. There were also more and larger starch granules in both the M
270 and BS chloroplasts in leaves of low light plants compared to the high light plants

271 (Figs. 4E-L, 5E-L; Tables 1, 2, 3). Grana width was significantly wider in BS
272 chloroplasts of two week-old high light *S. viridis* and M chloroplast of seven week-old
273 low light *S. viridis*, while there was no significant difference observed in grana
274 development between low light and high light-grown *Z. mays* (Figs. 4I-L, 5I-L; Tables
275 1, 2, 3).

276

277 **Plasmodesmata connections between mesophyll and bundle sheath**

278

279 Overall, there was significant growth irradiance, plant age, and interaction effect on
280 M-BS PD parameters in both *S. viridis* and *Z. mays* (Table 1). M-BS PD area per unit
281 leaf area in *S. viridis* leaves was four-fold greater in high light plants compared to low
282 light plants in seven-week old plants while in younger plants, low light plants had
283 greater M-BS PD area per unit leaf area (Fig. 6A; Table 1). In addition to lower BS
284 surface area per unit leaf area (S_b) (Fig. 6B), the reduction in M-BS PD area per unit
285 leaf area in seven-week old low light-grown *S. viridis* resulted from smaller pit fields
286 (Figs. 4M-P, 6C) populated by smaller PD (Fig. 6E), lower pit field area per unit cell
287 interface area (Figs. 4Q-T, 6I) and lower number of PD per unit cell interface area
288 (Fig. 6K). Meanwhile, bigger PD (Fig. 6E), greater pit field area per unit cell interface
289 area (Fig. 6I) and more PD per unit cell interface area (Fig. 6K) resulted in a greater
290 M-BS PD area per unit leaf area in two week-old low light *S. viridis*.

291

292 In two week-old *Z. mays*, high light plants had two-fold greater M-BS PD area per
293 unit leaf area compared to the low light plants while in older plants, this gap was
294 greatly reduced (Fig. 7A; Table 1). The smaller M-BS PD area per unit leaf area
295 discrepancy between low light and high light plants in older *Z. mays* was a result of
296 significantly smaller pit field size (Fig. 7C) and PD area (Fig. 7E) but greater pit field
297 area per unit cell interface area (Fig. 7I) and PD per unit cell interface area (Fig. 7K)
298 in low light plants. Meanwhile, lower PD connections between M and BS in leaves of
299 two-week old low light-grown *Z. mays* was a result of having fewer PD per unit pit
300 field area (Figs. 5M-P, 7G) and fewer pit fields (Figs. 5Q-T, 7I).

301

302 **Plasmodesmata connections between mesophyll**

303

304 Except for *S. viridis* M-M pit field area, there was significant growth irradiance, plant
305 age, and interaction effect in all M-M PD parameters in both *S. viridis* and *Z. mays*
306 (Table 1). In *S. viridis*, greater pit field area per unit cell interface area (Fig. 6J; Table
307 1) resulted to two-fold greater PD per unit cell interface area in high light plants
308 compared to low light plants (Fig. 6L; Table 1). Meanwhile, in two week-old *Z. mays*,
309 two-fold greater PD per unit cell interface area (Fig. 7L; Table 1) resulted from
310 having bigger PD (Fig. 7F), more PD per unit pit field area (Fig. 7H), and greater pit
311 field area per unit cell interface area (Fig. 7J) in high light plants compared to low
312 light plants. In older *Z. mays*, greater pit field area per unit cell interface area (Fig.
313 7J) resulted to greater PD per unit cell interface area in low light plants compared to
314 high light plants (Fig. 7L; Table 1).

315

316 **Discussion**

317

318 **The effect of growth irradiance on C₄ leaf PD density depends on plant age and** 319 **species**

320

321 Despite the suggestion that C₄ plants are less plastic than C₃ plants due to their
322 complex biochemical and anatomical attributes (Sage and McKown, 2006), there
323 have been numerous reports on C₄ species being capable of acclimation response
324 and plasticity to growth irradiance (Kromdijk et al., 2008; Pengelly et al., 2010;
325 Sonawane et al., 2018; Tazoe et al., 2008). Similarly, our results showed that when
326 NADP-ME species, *S. viridis* and *Z. mays*, were grown under different irradiances,
327 there was a species-specific difference and an overall significant plant age effect in
328 leaf PD density.

329

330 For a given plant developmental stage where the difference in M-BS PD area per
331 unit leaf area between low light-grown and high light-grown plants is at least two-fold
332 (as in seven-week old *S. viridis* and in two-week old *Z. mays*), there is also an
333 observed significant difference in BS chloroplasts content. This finding supports a
334 previous report (Wang et al., 2017) which suggested that chloroplast development
335 and function are strongly coordinated with PD function and formation in bundle
336 sheath cells (Brunkard et al., 2013). We also found that the overall lower M-BS PD
337 area per unit leaf area in low light-grown plants was largely attributed to impaired pit

338 field formation manifested by lower pit field coverage, smaller pit fields, and smaller
339 PD. It is believed that the primary PD formed during cytokinesis are pit field initials
340 (Giannoutsou et al., 2013) and that pit fields are formed as a result of primary PD
341 modification and/or secondary PD formation that happens later in development
342 (Ehlers and Kollmann, 2001; Faulkner et al., 2008). Addition of PD during primary
343 PD modification and/or secondary PD formation would entail resource and energy
344 costs which plants with more source leaves grown under non-limiting light could
345 energetically accommodate (Supplementary Fig. 2). On that same note, having thin
346 cell walls might also be an advantage for PD development. However, in this study
347 this is not supported as low light-grown plants which had thinner M and BS cell walls
348 also had fewer PD.

349

350 While it is not possible to make firm conclusions from only two species, it is tempting
351 to speculate that these two C₄ species may have evolved different acclimation
352 responses to low light associated with their C₄ lineage. *S. viridis* is a member of the
353 subtribe Cenchrinae of the MPC C₄ lineage while *Z. mays* is from the subtribe and C₄
354 lineage, Andropogoneae (GPWGII, 2012). This hypothesis agrees with the subtype-
355 dependent and species-specific responses observed in other growth irradiance
356 studies performed in C₄ plants. For instance, a previous comparison between *Z.*
357 *mays* and another NADP-ME C₄ grass, *Paspalum conjugatum* showed two different
358 responses to growth irradiance in terms of chlorophyll and Rubisco content, mainly
359 attributed to their different habitats (Ward and Woolhouse, 1986) but this could also
360 be due to C₄ lineage differences (GPWGII, 2012). Similarly, C₄ dicots belonging to
361 different subtypes, *Amaranthus cruentus* (NAD-ME) (Tazoe et al., 2006) and *Flaveria*
362 *bidentis* (NADP-ME) (Pengelly et al., 2010), showed contrasting responses to growth
363 irradiance in terms of chlorophyll content. It would be very interesting to see if
364 members of the same subtribe and/or C₄ lineage have similar patterns of leaf
365 phenotypic response to growth irradiance.

366

367 **There is not a tight link between PD density and photosynthetic capacity**

368

369 In this study, plant age had no effect on photosynthetic rates of the youngest fully
370 expanded leaves but there was an obvious difference in PD density between these
371 developmental stages. This observation, and the lack of correspondence between

372 PD density and photosynthetic flux under different growth irradiances, is summarised
373 in Figure 8. Here, the response of photosynthetic flux to incident light intensity is
374 calculated per M-BS interface PD at the two developmental stages and at the two
375 growth irradiances. If PD frequency was “adjusting” to photosynthetic flux, or indeed
376 limiting it, one might expect these light response curves to all be similar on a flux per
377 PD basis regardless of age or treatment. This is clearly not the case. One must
378 assume that these leaves are capable of maintaining M-BS fluxes of C₄ acids and C₃
379 products by tolerating considerable variation in diffusion gradients across this
380 interface and hence tolerate widely different levels of metabolites in the two
381 compartments (Hatch and Osmond, 1976). While it is difficult to directly measure
382 metabolite gradients in C₄ leaves, whole leaf metabolite measurements and recent
383 work using non-aqueous fractionation and stable isotope labelling (Arrivault et al.,
384 2017; Leegood and von Caemmerer, 1988) support this hypothesis. This is also true
385 when comparing C₄ species where PD densities between M and BS cells vary
386 between 5 and 12 PD μm^{-2} cell interface (Danila et al., 2018) despite these species
387 all having similar photosynthetic rates (Pinto et al., 2014).

388

389 **Light affects starch formation but not grana development in C₄ BS** 390 **chloroplasts**

391

392 In C₃ species, increased grana development is often observed in plants grown under
393 low light to maximise light capture under limiting environment (Björkman, 1981).
394 However, in this study, there was no overall enhancement in grana formation
395 observed in M or BS chloroplasts of low light plants. This could be because of the
396 complexity of the energy requirements of metabolism across the two cell types. It
397 has been proposed that plasticity in decarboxylation mechanism, the form of the C₄
398 acid transported to the BS and the shuttling of 3-PGA from the BS to the M
399 chloroplasts for reduction might all be ways in which energy balance could be
400 maintained under low irradiance in C₄ leaves (Furbank, 2011; Sharwood et al., 2014;
401 von Caemmerer and Furbank, 2016). Previous studies had also shown that when
402 NADP-ME type C₄ plants were grown under low light, the activity and protein
403 expression of both the decarboxylating enzyme NADP-ME (Sharwood et al., 2014;
404 Sonawane et al., 2018) and rubisco (Sharwood et al., 2014) were proportionally
405 reduced.

406
407
408
409
410
411
412
413
414
415
416
417
418
419
420
421
422
423
424
425
426
427
428
429
430
431
432
433
434
435
436
437
438
439

Meanwhile, accumulation of more and larger starch grains in the chloroplasts of low light *S. viridis* and *Z. mays* leaves were somewhat surprising as growth at low irradiance in most plants results in a reduction in starch levels (Zeeman et al., 2004). Our study, however, was not the first to show this as similar observations were also reported in low light-grown *Z. mays* and *Digitaria sanguinalis* from an independent study (Sowiński et al., 2007). Interestingly, these results were only observed in NADP-ME species but not in species belonging to NAD-ME or PCK subtypes (Sowiński et al., 2007). It is possible that the specialised metabolism of the NADP-ME type C₄ grasses plays a role in the availability of energy to fuel carbohydrate export from the bundle sheath or perhaps there are other unique biochemical features in the starch synthesis and degradation pathways in plants of this decarboxylation type (Ma et al., 2009; Russin et al., 1996; Slewinski et al., 2009).

Concluding Comments

The observation that PD density at the M-BS cell interface is greatly enhanced in C₄ leaves compared to C₃ leaves (Danila et al., 2016; Danila et al., 2018) to support C₄ photosynthetic metabolite flux would imply some functional relationship between PD density and photosynthetic capacity. While the data presented here indicate that there was some plasticity in PD density of C₄ leaves in response to growth irradiance, there was no clear correlation found between either photosynthetic capacity or photosynthetic flux and PD density at the M-BS cell interface. These results suggest a complex mechanism underlying the dynamic response of C₄ leaf PD formation to growth irradiance.

440 **References**

441

442 Arrivault, S., Obata, T., Szecówka, M., Mengin, V., Guenther, M., Hoehne, M.,
443 Fernie, A.R., Stitt, M., 2017. Metabolite pools and carbon flow during C₄
444 photosynthesis in maize: ¹³CO₂ labeling kinetics and cell type fractionation. *Journal*
445 *of Experimental Botany* 68, 283-298.

446 Björkman, O., 1981. Responses to Different Quantum Flux Densities, in: Lange,
447 O.L., Nobel, P.S., Osmond, C.B., Ziegler, H. (Eds.), *Physiological Plant Ecology I:*
448 *Responses to the Physical Environment.* Springer Berlin Heidelberg, Berlin,
449 Heidelberg, pp. 57-107.

450 Botha, C.E.J., 1992. Plasmodesmatal distribution, structure and frequency in relation
451 to assimilation in C₃ and C₄ grasses in southern Africa. *Planta* 187, 348-358.

452 Brunkard, J.O., Runkel, A.M., Zambryski, P.C., 2013. Plasmodesmata dynamics are
453 coordinated by intracellular signaling pathways. *Current opinion in plant biology* 16,
454 10.1016/j.pbi.2013.1007.1007.

455 Brutnell, T.P., Wang, L., Swartwood, K., Goldschmidt, A., Jackson, D., Zhu, X.-G.,
456 Kellogg, E., Van Eck, J., 2010. *Setaria viridis*: A Model for C(4) Photosynthesis. *The*
457 *Plant Cell* 22, 2537-2544.

458 Danila, F.R., Quick, W.P., White, R.G., Furbank, R.T., von Caemmerer, S., 2016.
459 The Metabolite Pathway between Bundle Sheath and Mesophyll: Quantification of
460 Plasmodesmata in Leaves of C(3) and C(4) Monocots. *The Plant Cell* 28, 1461-
461 1471.

462 Danila, F.R., Quick, W.P., White, R.G., Kelly, S., von Caemmerer, S., Furbank, R.T.,
463 2018. Multiple mechanisms for enhanced plasmodesmata density in disparate
464 subtypes of C₄ grasses. *Journal of Experimental Botany* 69, 1135-1145.

465 Ehlers, K., Kollmann, R., 2001. Primary and secondary plasmodesmata: structure,
466 origin, and functioning. *Protoplasma* 216, 1-30.

467 Faulkner, C., Akman, O.E., Bell, K., Jeffree, C., Oparka, K., 2008. Peeking into Pit
468 Fields: A Multiple Twinning Model of Secondary Plasmodesmata Formation in
469 Tobacco. *The Plant Cell* 20, 1504-1518.

470 Furbank, R., Jenkins, C., Hatch, M., 1990. C₄ Photosynthesis:
471 Quantum Requirement, C₄ acid overcycling and *Q*-Cycle
472 Involvement. *Functional Plant Biology* 17, 1-7.

473 Furbank, R.T., 2011. Evolution of the C₄ photosynthetic mechanism: are there really
474 three C₄ acid decarboxylation types? *Journal of Experimental Botany* 62, 3103-
475 3108.

476 Giannoutsou, E., Sotiriou, P., Apostolakos, P., Galatis, B., 2013. Early local
477 differentiation of the cell wall matrix defines the contact sites in lobed mesophyll cells
478 of *Zea mays*. *Annals of Botany* 112, 1067-1081.

- 479 GPWGII, 2012. New grass phylogeny resolves deep evolutionary relationships and
480 discovers C₄ origins. *New Phytologist* 193, 304-312.
- 481 Gunning, B.E.S., 1978. Age-related and origin-related control of the numbers of
482 plasmodesmata in cell walls of developing *Azolla* roots. *Planta* 143, 181-190.
- 483 Hatch, M.D., 1987. C₄ photosynthesis: a unique blend of modified biochemistry,
484 anatomy and ultrastructure. *Biochimica et Biophysica Acta (BBA) - Reviews on*
485 *Bioenergetics* 895, 81-106.
- 486 Hatch, M.D., Osmond, C.B., 1976. Compartmentation and Transport in C₄
487 Photosynthesis, in: Stocking, C.R., Heber, U. (Eds.), *Transport in Plants III*. Springer
488 Berlin Heidelberg, pp. 144-184.
- 489 Henderson, S., Caemmerer, S., Farquhar, G., 1992. Short-Term Measurements of
490 Carbon Isotope Discrimination in Several C₄ Species. *Functional Plant*
491 *Biology* 19, 263-285.
- 492 Kromdijk, J., Schepers, H.E., Albanito, F., Fitton, N., Carroll, F., Jones, M.B., Finnan,
493 J., Lanigan, G.J., Griffiths, H., 2008. Bundle Sheath Leakiness and Light Limitation
494 during C₄ Leaf and Canopy CO₂ Uptake. *Plant*
495 *Physiology* 148, 2144-2155.
- 496 Leegood, R.C., von Caemmerer, S., 1988. The relationship between contents of
497 photosynthetic metabolites and the rate of photosynthetic carbon assimilation in
498 leaves of *Amaranthus edulis* L. *Planta* 174, 253-262.
- 499 Li, P., Brutnell, T.P., 2011. *Setaria viridis* and *Setaria italica*, model genetic systems
500 for the Panicoid grasses. *Journal of Experimental Botany* 62, 3031-3037.
- 501 Lu, K.J., Danila, F.R., Cho, Y., Faulkner, C., 2018. Peeking at a plant through the
502 holes in the wall – exploring the roles of plasmodesmata. *New Phytologist* 0.
- 503 Ma, Y., Slewinski, T.L., Baker, R.F., Braun, D.M., 2009. Tie-dyed1 Encodes a Novel,
504 Phloem-Expressed Transmembrane Protein That Functions in Carbohydrate
505 Partitioning. *Plant Physiology* 149, 181-194.
- 506 Pengelly, J.J.L., Sirault, X.R.R., Tazoe, Y., Evans, J.R., Furbank, R.T., von
507 Caemmerer, S., 2010. Growth of the C₄ dicot *Flaveria bidentis*: photosynthetic
508 acclimation to low light through shifts in leaf anatomy and biochemistry. *Journal of*
509 *Experimental Botany* 61, 4109-4122.
- 510 Pinto, H., Sharwood, R.E., Tissue, D.T., Ghannoum, O., 2014. Photosynthesis of
511 C(3), C(3)-C(4), and C(4) grasses at glacial CO(2). *Journal of Experimental Botany*
512 65, 3669-3681.
- 513 Porra, R.J., Thompson, W.A., Kriedemann, P.E., 1989. Determination of accurate
514 extinction coefficients and simultaneous equations for assaying chlorophylls a and b
515 extracted with four different solvents: verification of the concentration of chlorophyll
516 standards by atomic absorption spectroscopy. *Biochimica et Biophysica Acta (BBA) -*
517 *Bioenergetics* 975, 384-394.

518 Russin, W.A., Evert, R.F., Vanderveer, P.J., Sharkey, T.D., Briggs, S.P., 1996.
519 Modification of a Specific Class of Plasmodesmata and Loss of Sucrose Export
520 Ability in the sucrose export defective1 Maize Mutant. *The Plant Cell* 8, 645-658.

521 Sage, R.F., McKown, A.D., 2006. Is C₄ photosynthesis less phenotypically plastic
522 than C₃ photosynthesis?*. *Journal of Experimental Botany* 57, 303-317.

523 Sage, R.F., Pearcy, R.W., 2000. The Physiological Ecology of C₄ Photosynthesis, in:
524 Leegood, R.C., Sharkey, T.D., von Caemmerer, S. (Eds.), *Photosynthesis:*
525 *Physiology and Metabolism*. Springer Netherlands, Dordrecht, pp. 497-532.

526 Seagull, R.W., 1983. Differences in the frequency and disposition of plasmodesmata
527 resulting from root cell elongation. *Planta* 159, 497-504.

528 Sharwood, R.E., Sonawane, B.V., Ghannoum, O., 2014. Photosynthetic flexibility in
529 maize exposed to salinity and shade. *Journal of Experimental Botany* 65, 3715-3724.

530 Slewinski, T.L., Meeley, R., Braun, D.M., 2009. Sucrose transporter1 functions in
531 phloem loading in maize leaves. *Journal of Experimental Botany* 60, 881-892.

532 Sonawane, B.V., Sharwood, R.E., Whitney, S., Ghannoum, O., 2018. Shade
533 compromises the photosynthetic efficiency of NADP-ME less than that of PEP-CK
534 and NAD-ME C₄ grasses. *Journal of Experimental Botany* 69, 3053-3068.

535 Sowiński, P., Bilska, A., Barańska, K., Fronk, J., Kobus, P., 2007. Plasmodesmata
536 density in vascular bundles in leaves of C₄ grasses grown at different light conditions
537 in respect to photosynthesis and photosynthate export efficiency. *Environmental and*
538 *Experimental Botany* 61, 74-84.

539 Tangl, E., 1879. ober offene Kommunikation zwischen den Zellen des Endosperms
540 einiger Samen. *Jb Wiss Bot* 12, 170-190.

541 Tazoe, Y., Hanba, Y.T., Furumoto, T., Noguchi, K., Terashima, I., 2008.
542 Relationships Between Quantum Yield for CO₂ Assimilation, Activity of Key
543 Enzymes and CO₂ Leakiness in *Amaranthus cruentus*, a C₄ Dicot, Grown in High or
544 Low Light. *Plant and Cell Physiology* 49, 19-29.

545 Tazoe, Y., Noguchi, K., Terashima, I., 2006. Effects of growth light and nitrogen
546 nutrition on the organization of the photosynthetic apparatus in leaves of a C₄ plant,
547 *Amaranthus cruentus*. *Plant, Cell & Environment* 29, 691-700.

548 von Caemmerer, S., Furbank, R., 2003. The C₄ pathway: an efficient CO₂ pump.
549 *Photosynthesis Research* 77, 191-207.

550 von Caemmerer, S., Furbank, R.T., 2016. Strategies for improving C₄
551 photosynthesis. *Current Opinion in Plant Biology* 31, 125-134.

552 Wang, P., Khoshraves, R., Karki, S., Tapia, R., Balahadia, C.P., Bandyopadhyay,
553 A., Quick, W.P., Furbank, R.T., Sage, T.L., Langdale, J.A., 2017. Re-creation of a
554 key step in the evolutionary switch from C₃ to C₄ leaf anatomy. *Current Biology* 27,
555 3278-3287.

556 Ward, D.A., Woolhouse, H.W., 1986. Comparative effects of light during growth on
557 the photosynthetic properties of NADP-ME type C₄ grasses from open and shaded

558 habitats. I. Gas exchange, leaf anatomy and ultrastructure*. Plant, Cell &
559 Environment 9, 261-270.

560 Zeeman, S.C., Smith, S.M., Smith, A.M., 2004. The breakdown of starch in leaves.
561 New Phytologist 163, 247-261.

562

563

564

565

566

567

568

569

570

571

572

573

574

575

576

577

578

579

580

581

582

583

584

585

586

587

588

589

590

591

592 **Figure legends**

593

594 **Figure 1.** Light response curves of gross CO₂ assimilation of *Setaria viridis* (A) and
595 *Zea mays* (B) grown under different irradiances. High light (HL) at 1000 μmol m⁻² s⁻¹
596 and low light (LL) at 100 μmol m⁻² s⁻¹. Photosynthetic measurement was done on the
597 middle portion of the youngest fully expanded leaf of plants at two weeks (2w) and
598 seven weeks after germination (7w) plants. Gross CO₂ assimilation rates of *S. viridis*
599 and *Z. mays* measured at growth irradiances are plotted in (C) and (D), respectively.
600 Each symbol or bar represents the mean ± SE, n=3. Letters indicate the ranking
601 (lowest=a) using multiple-comparison Tukey's post-hoc test. Bars with same letter
602 are not statistically different at P<0.05. Mean dark respiration rates and
603 corresponding statistical analysis were provided in Supplementary Figure 3 and
604 Table 1, respectively.

605

606 **Figure 2.** Leaf properties of *S. viridis* grown under different irradiances. Low light at
607 100 μmol m⁻² s⁻¹ and high light at 1000 μmol m⁻² s⁻¹. Embedded values on (C)
608 correspond to chlorophyll a/b ratio. All measurements were done using the middle
609 portion of the youngest fully expanded leaf harvested immediately after gas
610 exchange measurement. Letters indicate the ranking (lowest=a) using multiple-
611 comparison Tukey's post-hoc test. Bars with same letter are not statistically different
612 at P<0.05. N, nitrogen; BS, bundle sheath; M, mesophyll.

613

614 **Figure 3.** Leaf properties of *Z. mays* grown under different irradiances. Details and
615 statistics are as described in Fig. 2.

616

617 **Figure 4.** Leaf micrographs of *S. viridis* grown under different irradiances. Low light
618 at 100 μmol m⁻² s⁻¹ and high light at 1000 μmol m⁻² s⁻¹. Light micrographs (A-D) were
619 generated using the middle portion of the youngest fully expanded leaf harvested
620 immediately after gas exchange measurement. Corresponding transmission electron
621 micrographs (TEM) of bundle sheath (BS) chloroplasts (E-H) and mesophyll (M)
622 chloroplasts (I-L) were obtained. Pit field size (white outline in scanning electron
623 micrographs (SEM)) (M-P) and pit field (green fluorescence in confocal micrographs)
624 distribution (Q-T) between M and BS were also shown. s, starch grain. Light

625 micrograph bars = 25 μm . TEM bars = 1 μm , confocal micrograph bars = 10 μm ,
626 SEM bars = 0.5 μm .

627

628 **Figure 5.** Leaf micrographs of *Z. mays* grown under different irradiances. Details are
629 as described in Fig. 4.

630

631 **Figure 6.** Leaf plasmodesmata (PD) properties of *S. viridis* grown under different
632 irradiances. Low light at 100 $\mu\text{mol m}^{-2} \text{s}^{-1}$ and high light at 1000 $\mu\text{mol m}^{-2} \text{s}^{-1}$. All
633 measurements were done using the middle portion of the youngest fully expanded
634 leaf harvested immediately after gas exchange measurement. Letters indicate the
635 ranking (lowest=a) using multiple-comparison Tukey's post-hoc test. Bars with same
636 letter are not statistically different at $P < 0.05$. M, mesophyll; BS, bundle sheath; S_b ,
637 bundle sheath surface area per leaf unit area.

638

639 **Figure 7.** Leaf plasmodesmata (PD) properties of *Z. mays* grown under different
640 irradiances. Details and statistics are as described in Fig. 6.

641

642 **Figure 8.** Light response curves of plasmodesmata (PD) flux between mesophyll
643 and bundle sheath cells of *S. viridis* (A) and *Z. mays* (B) grown under different
644 irradiances. Calculations as previously described in (Danila et al., 2016). Gross CO_2
645 assimilation rate per PD assumes that in C_4 species the minimum flux of C_4 acids
646 through the PD needs to be equal to or greater than the gross CO_2 assimilation rate
647 (Henderson et al., 1992). See Figure 1 for details.

648

649 **Supplementary Figure 1.** Relationship between gross CO_2 assimilation rate and
650 total leaf N content of *S. viridis* and *Z. mays* grown under different irradiances. Low
651 light (LL) at 100 $\mu\text{mol m}^{-2} \text{s}^{-1}$ and high light (HL) at 1000 $\mu\text{mol m}^{-2} \text{s}^{-1}$.

652

653 **Supplementary Figure 2.** Seven week-old *S. viridis* and *Z. mays* grown under
654 different irradiances. Low light at 100 $\mu\text{mol m}^{-2} \text{s}^{-1}$ and high light at 1000 $\mu\text{mol m}^{-2} \text{s}^{-1}$.
655 (A) Low light-grown *S. viridis*, (B) high light-grown *S. viridis*, (C) low light-grown *Z.*
656 *mays*, and (D) high light-grown *Z. mays*. Red arrowhead points to the leaf used for
657 measurements and quantification. Bar = 20 cm.

658
659
660
661
662
663
664
665
666
667
668
669
670
671
672
673
674
675
676
677
678
679
680
681
682
683
684
685
686
687
688
689
690
691

Supplementary Figure 3. Dark respiration rates of *S. viridis* (A) and *Z. mays* (B) grown under different growth irradiances. Each bar represents the mean \pm SE, n=3. Letters indicate the ranking (lowest=a) using multiple-comparison Tukey's post-hoc test. Bars with same letter are not statistically different at $P<0.05$.

692 **Tables**

693

694 **Table 1.** Summary of statistical analysis using two-way ANOVA to test for the effects
 695 of growth irradiance and plant age to various response parameters.

Parameter	<i>S. viridis</i>			<i>Z. mays</i>		
	Irradiance	Age	Irradiance x Age	Irradiance	Age	Irradiance x Age
A _{gross} (μmol CO ₂ m ⁻² s ⁻¹)	***	ns	ns	***	**	*
R _d (μmol CO ₂ m ⁻² s ⁻¹)	**	*	ns	***	**	ns
LMA (g m ⁻²)	***	**	ns	***	***	***
Total leaf N (mmol m ⁻²)	***	ns	ns	***	***	**
Chl a+b (μmol m ⁻²)	**	**	ns	*	*	ns
Chl a/b	***	*	ns	***	ns	***
BS chloroplast content (%)	ns	***	*	*	ns	ns
BS chloroplast size (μm ²)	ns	ns	***	***	**	***
M chloroplast size (μm ²)	ns	***	ns	***	ns	ns
BS grana width (μm)	ns	ns	**	ns	*	ns
M grana width (μm)	**	***	***	*	***	ns
BS starch granule per chloroplast	***	***	***	***	ns	ns
M starch granule per chloroplast	***	***	***	*	*	*
BS starch granule size (μm ²)	***	***	***	***	ns	***
M starch granule size (μm ²)	***	***	***	***	***	***
Vein circumference (μm)	***	ns	***	***	ns	***
Interveinal distance (μm)	***	ns	***	***	***	*
Leaf thickness (μm)	***	*	***	***	ns	***
BS cell wall thickness (μm)	***	ns	ns	***	***	***
M cell wall thickness (μm)	***	**	ns	***	**	ns
S _b (m ² m ⁻²)	***	***	**	ns	**	ns
M-BS PD area per unit leaf area (m ² m ⁻²)	***	***	***	***	***	***
M-BS pit field area (μm ²)	**	ns	**	**	**	ns
M-M pit field area (μm ²)	ns	ns	ns	*	ns	***
M-BS PD area (μm ²)	ns	***	***	**	***	***
M-M PD area (μm ²)	ns	***	*	***	*	***
M-BS PD per unit pit field area (PD μm ⁻²)	***	***	***	***	ns	***
M-M PD per unit pit field area (PD μm ⁻²)	***	***	***	***	***	***
M-BS pit field area per cell interface area (%)	***	***	***	***	**	***
M-M pit field area per cell interface area (%)	***	***	***	ns	***	***
M-BS PD per unit cell interface area (PD μm ⁻²)	***	***	***	***	ns	***
M-M PD per unit cell interface area (PD μm ⁻²)	***	***	***	***	***	***

696

697 ns, not significant ($P>0.05$); * $P<0.05$; ** $P<0.01$; *** $P<0.001$. A_{gross}, gross CO₂
 698 assimilation rate; R_d, dark respiration rate; LMA, leaf mass per area; Chl, chlorophyll;
 699 BS, bundle sheath; M, mesophyll; S_b, bundle sheath surface area per unit leaf area;
 700 PD, plasmodesmata.

701

702 **Table 2.** Chloroplast properties of *S. viridis* grown under low ($100 \mu\text{mol m}^{-2} \text{s}^{-1}$) and
 703 high ($1000 \mu\text{mol m}^{-2} \text{s}^{-1}$) irradiances.

704

Parameter	<i>S. viridis</i>			
	2-week old		7-week old	
	Low	High	Low	High
BS chloroplast size (μm^2), n=39	$19.6 \pm 1.07^{\text{ab}}$	$25.6 \pm 1.76^{\text{c}}$	$22.8 \pm 1.52^{\text{bc}}$	$16.5 \pm 1.73^{\text{a}}$
M chloroplast size (μm^2), n=12	$21.2 \pm 1.93^{\text{ab}}$	$25.2 \pm 2.46^{\text{b}}$	$16.6 \pm 1.71^{\text{a}}$	$15.9 \pm 1.33^{\text{a}}$
BS grana width (μm), n=47	$0.09 \pm 0.007^{\text{a}}$	$0.12 \pm 0.004^{\text{b}}$	$0.11 \pm 0.009^{\text{ab}}$	$0.10 \pm 0.004^{\text{b}}$
M grana width (μm), n=120	$0.32 \pm 0.012^{\text{a}}$	$0.33 \pm 0.014^{\text{a}}$	$0.45 \pm 0.024^{\text{b}}$	$0.35 \pm 0.015^{\text{a}}$
BS starch granule per chloroplast, n=39	$15 \pm 1.1^{\text{b}}$	$6 \pm 0.4^{\text{a}}$	$5 \pm 0.5^{\text{a}}$	$4 \pm 0.4^{\text{a}}$
M starch granule per chloroplast, n=12	$8 \pm 0.9^{\text{b}}$	$1 \pm 0.4^{\text{a}}$	$2 \pm 0.5^{\text{a}}$	$0 \pm 0.0^{\text{a}}$
BS starch granule size (μm^2), n=125	$0.27 \pm 0.007^{\text{c}}$	$0.08 \pm 0.003^{\text{a}}$	$0.15 \pm 0.006^{\text{b}}$	$0.06 \pm 0.003^{\text{a}}$
M starch granule size (μm^2), n=25	$0.33 \pm 0.021^{\text{b}}$	$0.07 \pm 0.005^{\text{a}}$	$0.05 \pm 0.007^{\text{a}}$	na

705

706 The average number of corresponding structures measured is indicated by n. Letters
 707 indicate the ranking (lowest=a) of plants within each single row using multiple-
 708 comparison Tukey's post-hoc test. Values followed by the same superscript letter are
 709 not significantly different at the 5% level. BS, bundle sheath; M, mesophyll; na, not
 710 applicable.

711

712

713

714

715

716

717

718

719

720

721

722

723

724

725

726 **Table 3.** Chloroplast properties of *Z. mays* grown under low ($100 \mu\text{mol m}^{-2} \text{s}^{-1}$) and
 727 high ($1000 \mu\text{mol m}^{-2} \text{s}^{-1}$) irradiances.

728

Parameter	<i>Z. mays</i>			
	2-week old		7-week old	
	Low	High	Low	High
BS chloroplast size (μm^2), n=56	8.9 ± 0.44^a	12.5 ± 0.78^b	8.3 ± 0.39^a	17.4 ± 0.91^c
M chloroplast size (μm^2), n=30	10.8 ± 1.13^a	16.3 ± 1.13^b	11.4 ± 0.82^{ac}	15.2 ± 0.99^{bc}
BS grana width (μm), n=28	0.07 ± 0.003^a	0.07 ± 0.003^a	0.08 ± 0.006^a	0.08 ± 0.005^a
M grana width (μm), n=130	0.43 ± 0.014^a	0.49 ± 0.019^{ab}	0.54 ± 0.035^{bc}	0.58 ± 0.026^c
BS starch granule per chloroplast, n=56	4 ± 0.5^a	1 ± 0.3^b	4 ± 0.4^a	0 ± 0.0^b
M starch granule per chloroplast, n=30	0 ± 0.0^a	0 ± 0.0^a	1 ± 0.4^b	0 ± 0.0^a
BS starch granule size (μm^2), n=107	0.12 ± 0.005^a	0.07 ± 0.012^a	0.15 ± 0.005^b	na
M starch granule size (μm^2), n=34	na	na	0.09 ± 0.008^b	na

729

730 The average number of corresponding structures measured is indicated by n. Letters
 731 indicate the ranking (lowest=a) of plants within each single row using multiple-
 732 comparison Tukey's post-hoc test. Values followed by the same superscript letter are
 733 not significantly different at the 5% level. BS, bundle sheath; M, mesophyll; na, not
 734 applicable.

Figures

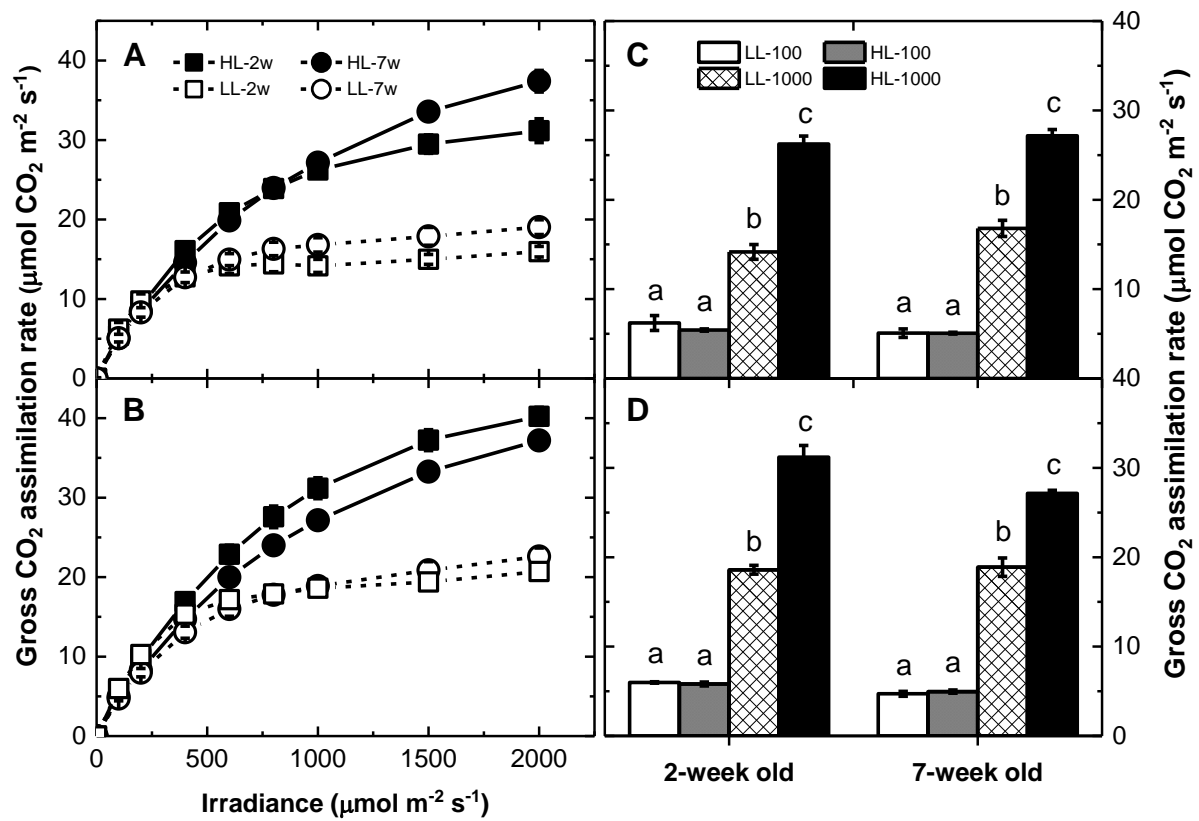


Figure 1. Light response curves of gross CO₂ assimilation of *Setaria viridis* (A) and *Zea mays* (B) grown under different irradiances. High light (HL) at 1000 $\mu\text{mol m}^{-2} \text{s}^{-1}$ and low light (LL) at 100 $\mu\text{mol m}^{-2} \text{s}^{-1}$. Photosynthetic measurement was done on the middle portion of the youngest fully expanded leaf of plants at two weeks (2w) and seven weeks after germination (7w) plants. Gross CO₂ assimilation rates of *S. viridis* and *Z. mays* measured at growth irradiances are plotted in (C) and (D), respectively. Each symbol or bar represents the mean \pm SE, n=3. Letters indicate the ranking (lowest=a) using multiple-comparison Tukey's post-hoc test. Bars with same letter are not statistically different at $P < 0.05$. Mean dark respiration rates and corresponding statistical analysis were provided in Supplementary Figure 3 and Table 1, respectively.

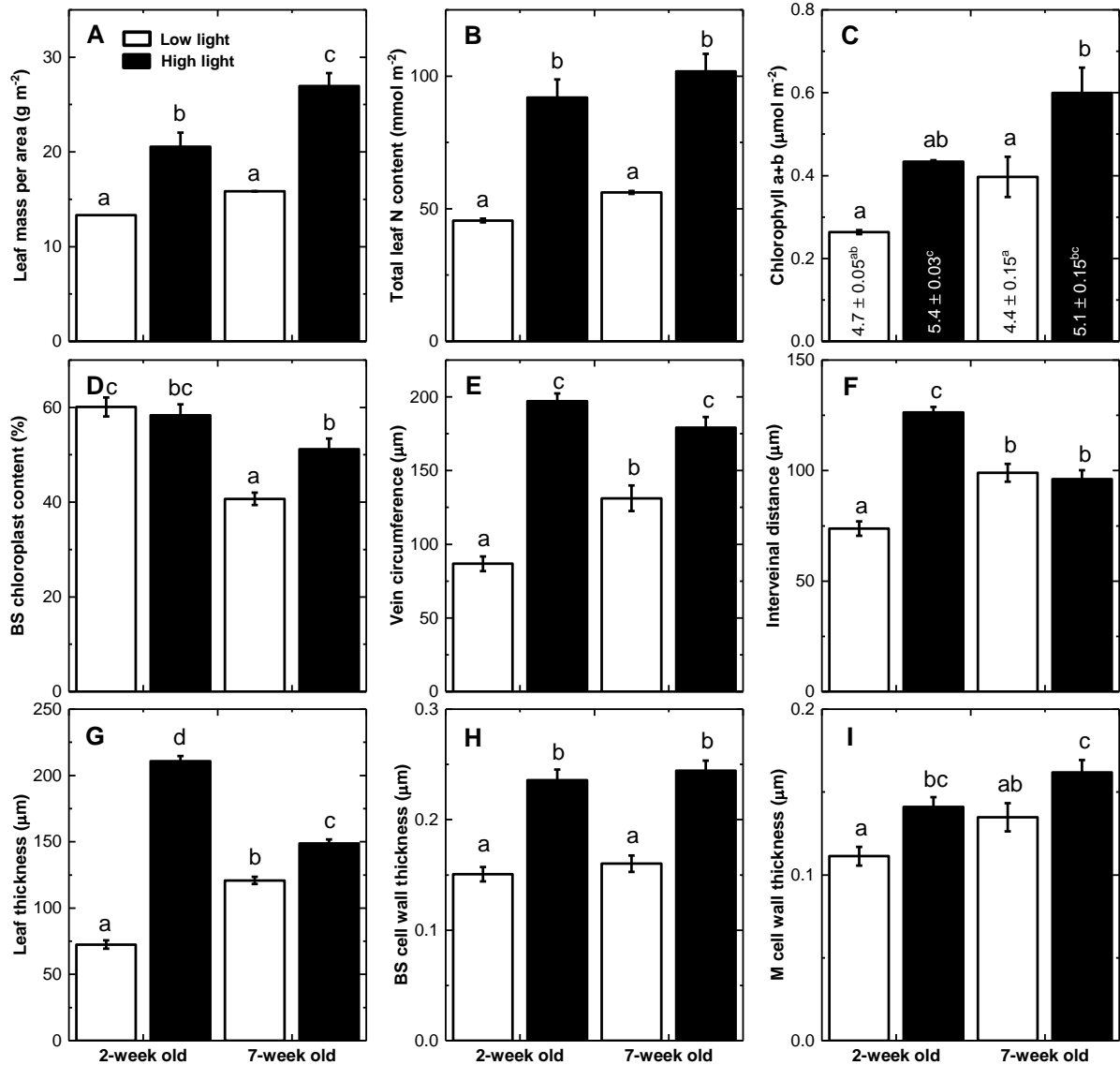


Figure 2. Leaf properties of *S. viridis* grown under different irradiances. Low light at $100 \mu\text{mol m}^{-2} \text{s}^{-1}$ and high light at $1000 \mu\text{mol m}^{-2} \text{s}^{-1}$. Embedded values on (C) correspond to chlorophyll a/b ratio. All measurements were done using the middle portion of the youngest fully expanded leaf harvested immediately after gas exchange measurement. Letters indicate the ranking (lowest=a) using multiple-comparison Tukey's post-hoc test. Bars with same letter are not statistically different at $P < 0.05$. N, nitrogen; BS, bundle sheath; M, mesophyll.

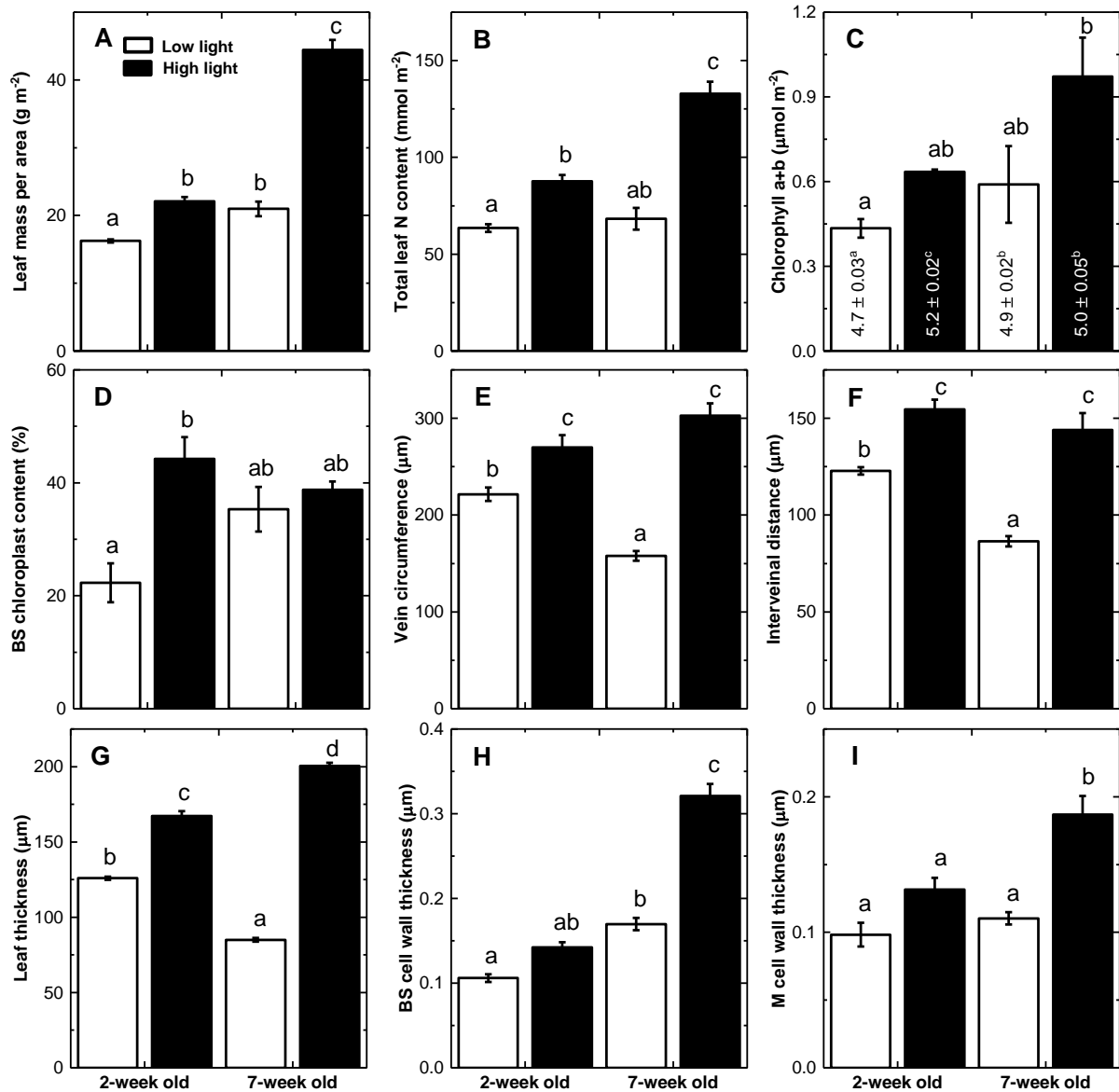


Figure 3. Leaf properties of *Z. mays* grown under different irradiances. Details and statistics are as described in Fig. 2.

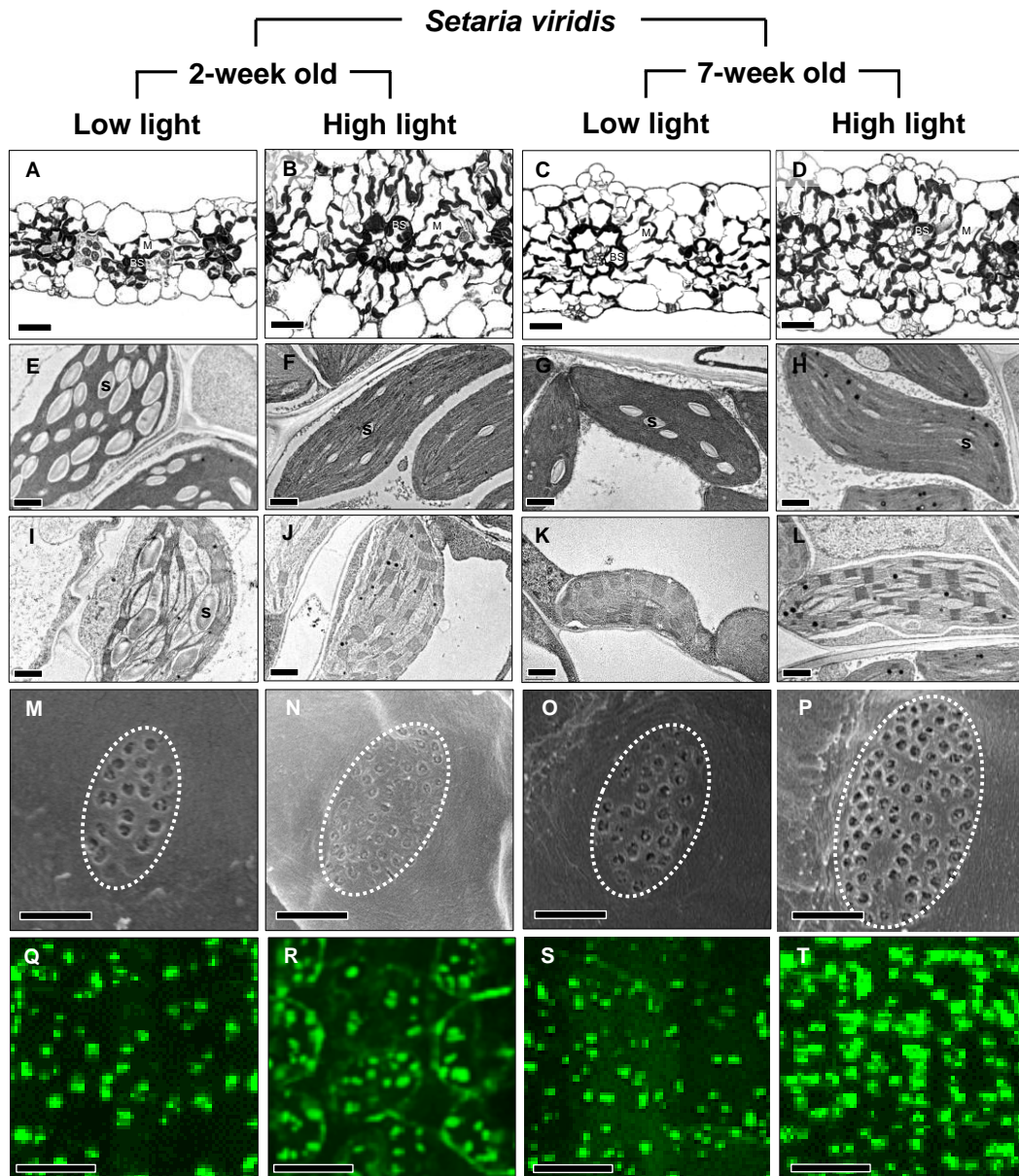


Figure 4. Leaf micrographs of *S. viridis* grown under different irradiances. Low light at $100 \mu\text{mol m}^{-2} \text{s}^{-1}$ and high light at $1000 \mu\text{mol m}^{-2} \text{s}^{-1}$. Light micrographs (A-D) were generated using the middle portion of the youngest fully expanded leaf harvested immediately after gas exchange measurement. Corresponding transmission electron micrographs (TEM) of bundle sheath (BS) chloroplasts (E-H) and mesophyll (M) chloroplasts (I-L) were obtained. Pit field size (white outline in scanning electron micrographs (SEM)) (M-P) and pit field (green fluorescence in confocal micrographs) distribution (Q-T) between M and BS were also shown. s, starch grain. Light micrograph bars = $25 \mu\text{m}$. TEM bars = $1 \mu\text{m}$, confocal micrograph bars = $10 \mu\text{m}$, SEM bars = $0.5 \mu\text{m}$.

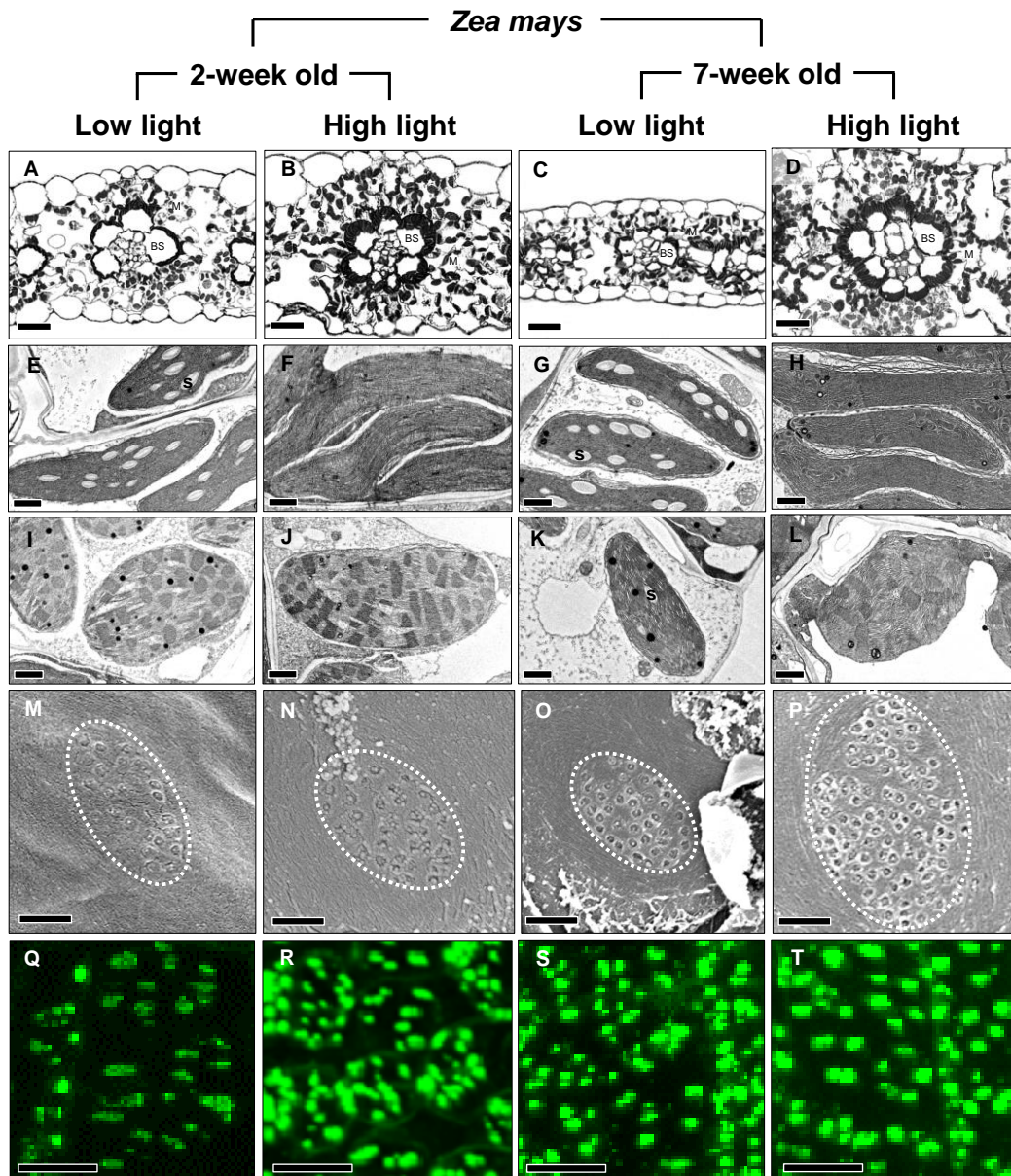


Figure 5. Leaf micrographs of *Z. mays* grown under different irradiances. Details are as described in Fig. 4.

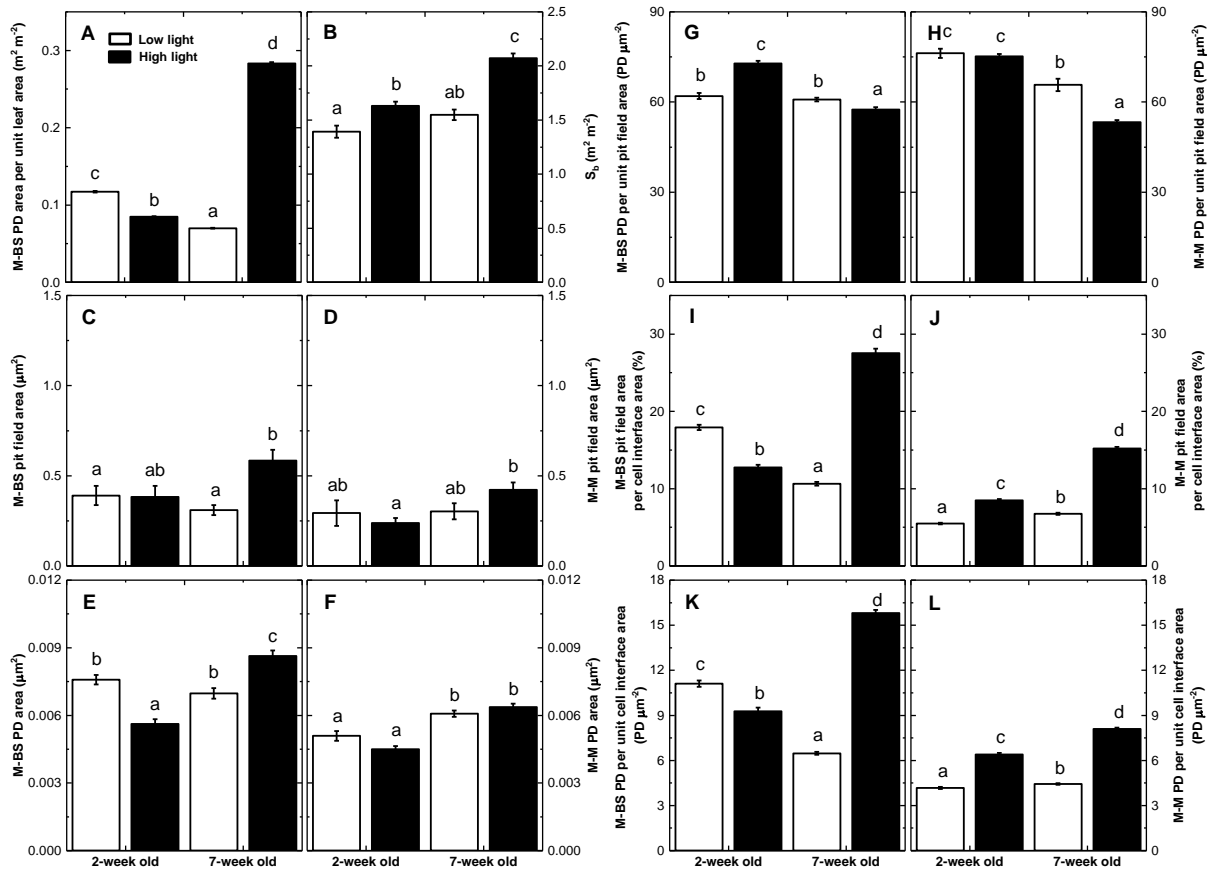


Figure 6. Leaf plasmodesmata (PD) properties of *S. viridis* grown under different irradiances. Low light at $100 \mu\text{mol m}^{-2} \text{s}^{-1}$ and high light at $1000 \mu\text{mol m}^{-2} \text{s}^{-1}$. All measurements were done using the middle portion of the youngest fully expanded leaf harvested immediately after gas exchange measurement. Letters indicate the ranking (lowest=a) using multiple-comparison Tukey's post-hoc test. Bars with same letter are not statistically different at $P < 0.05$. M, mesophyll; BS, bundle sheath; S_b , bundle sheath surface area per leaf unit area.

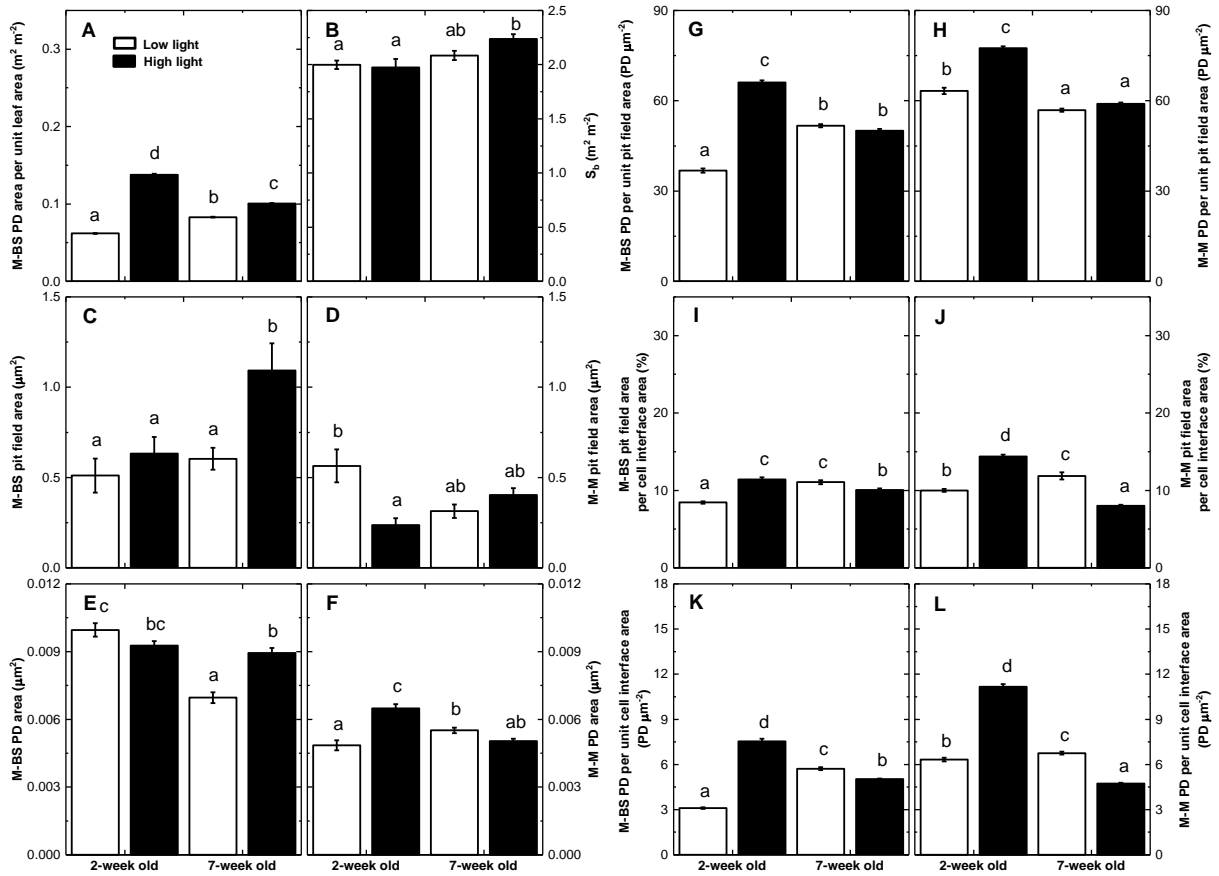


Figure 7. Leaf plasmodesmata (PD) properties of *Z. mays* grown under different irradiances. Details and statistics are as described in Fig. 6.

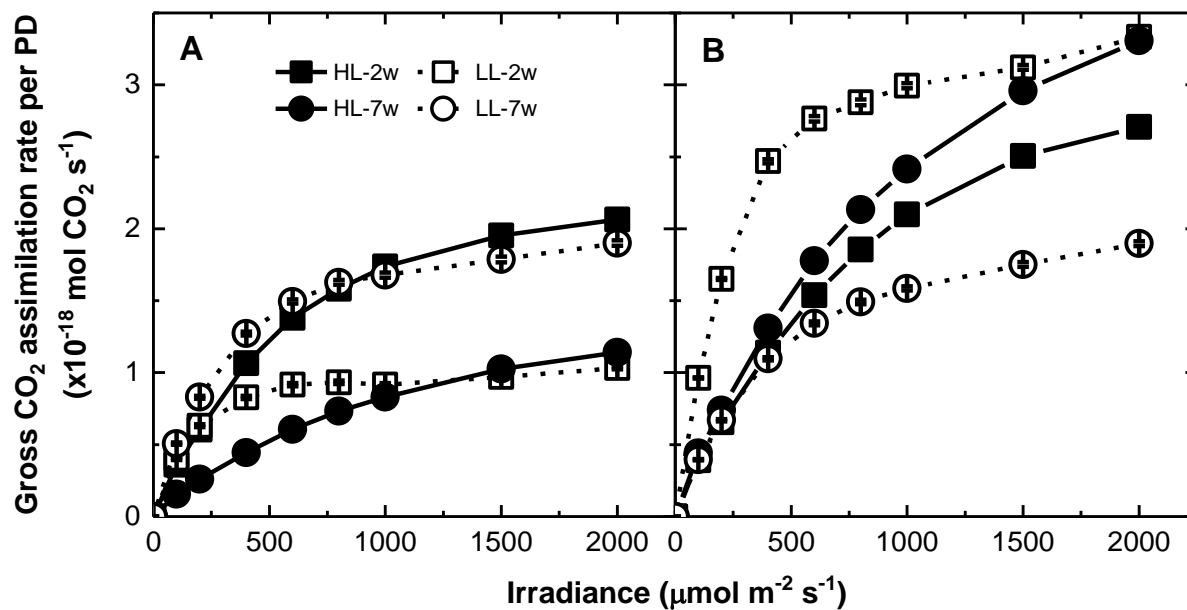
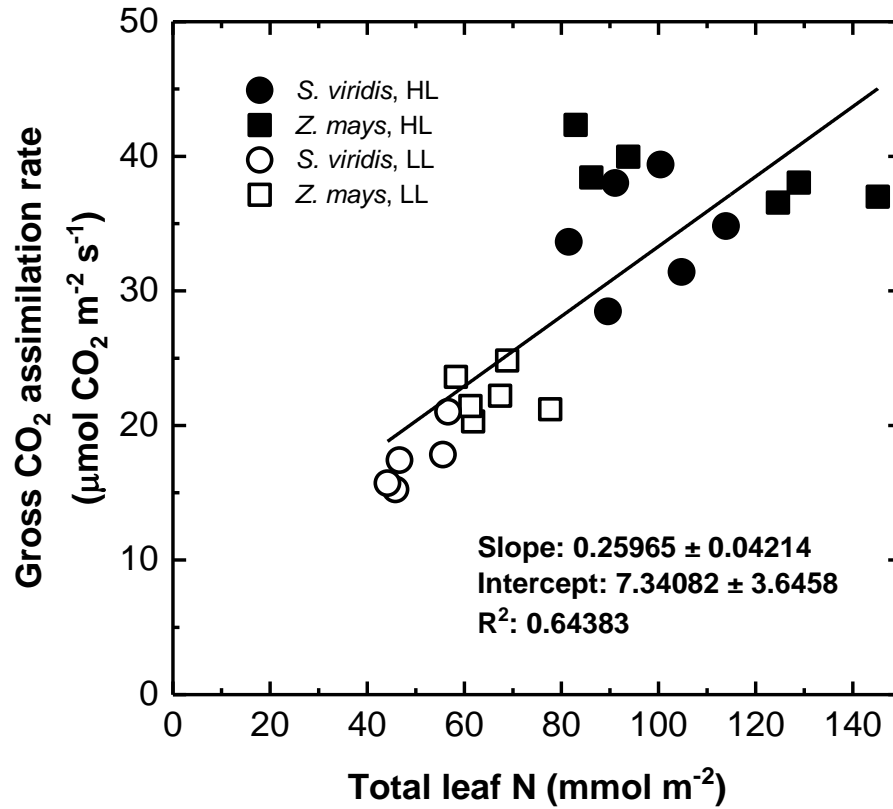
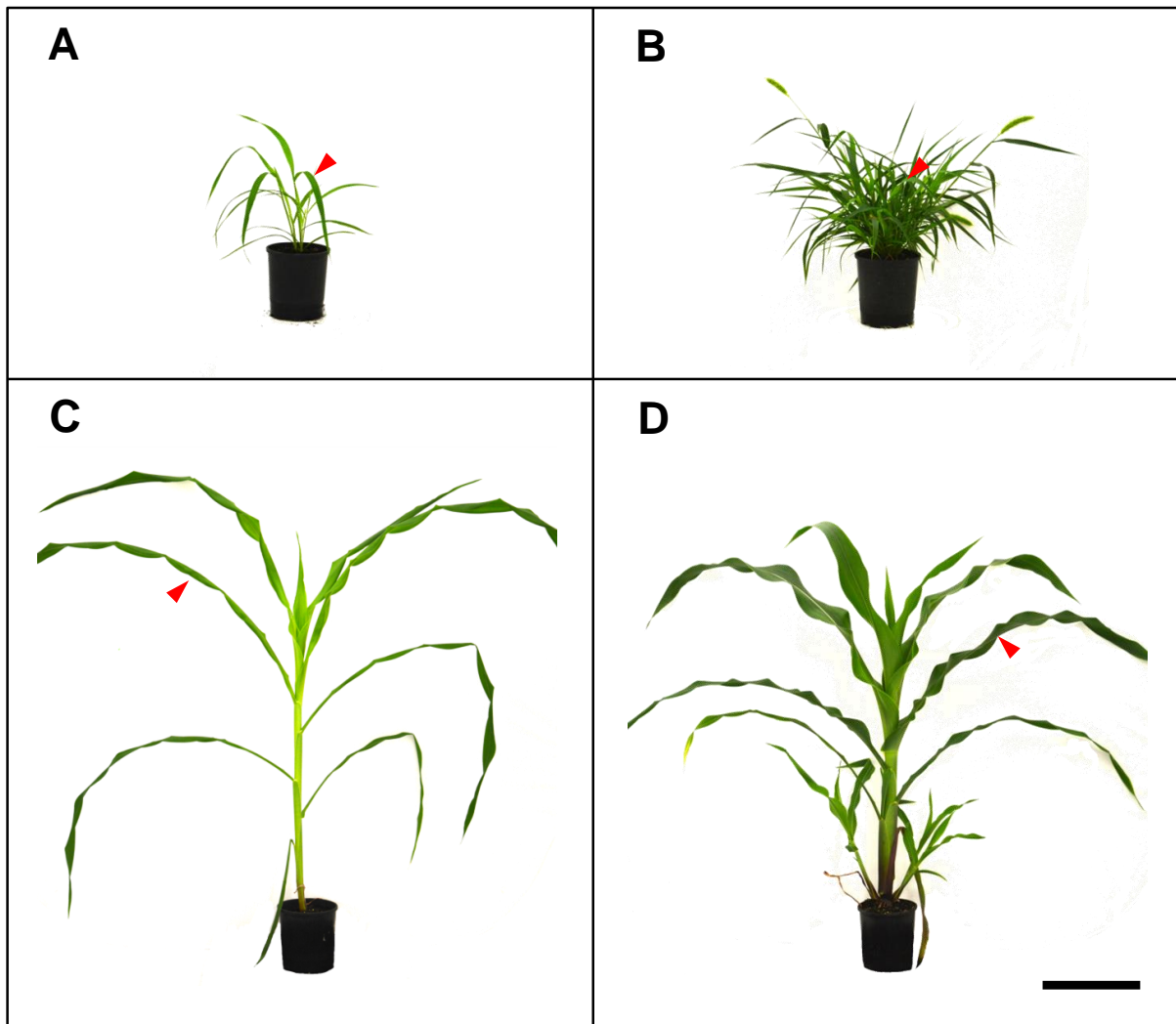


Figure 8. Light response curves of plasmodesmata (PD) flux between mesophyll and bundle sheath cells of *S. viridis* (A) and *Z. mays* (B) grown under different irradiances. Calculations as previously described in (Danila et al., 2016). Gross CO₂ assimilation rate per PD assumes that in C₄ species the minimum flux of C₄ acids through the PD needs to be equal to or greater than the gross CO₂ assimilation rate (Henderson et al., 1992). See Figure 1 for details.

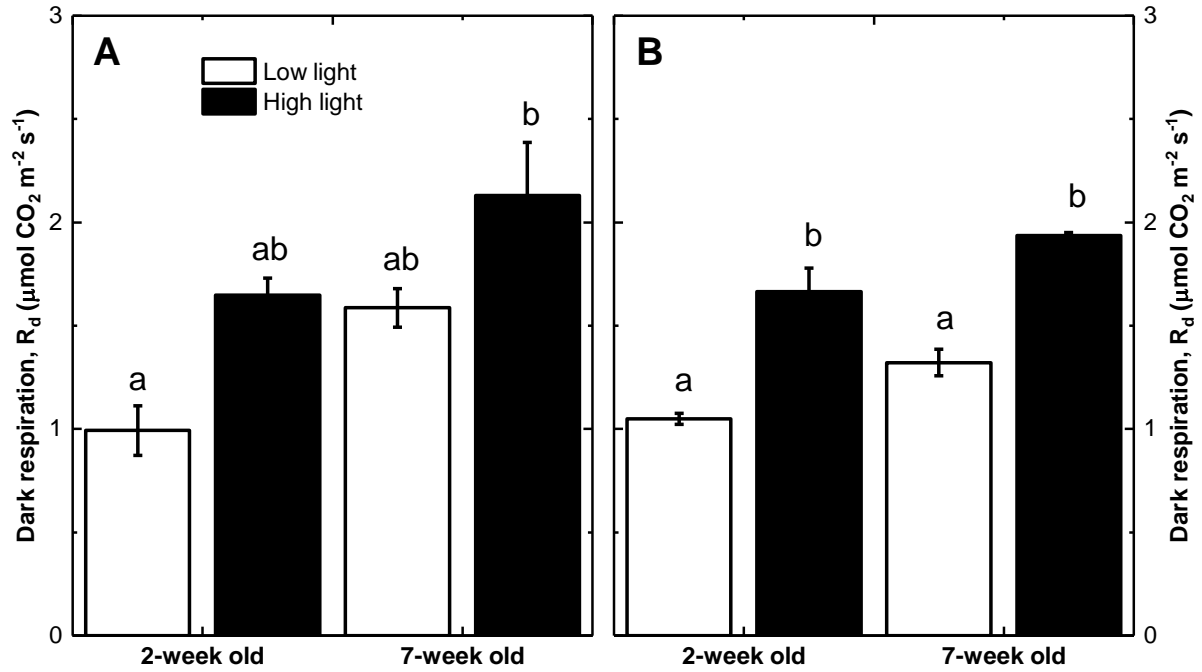
Supporting information



Supplementary Figure 1. Relationship between gross CO₂ assimilation rate and total leaf N content of *S. viridis* and *Z. mays* grown under different irradiances. Low light (LL) at $100 \mu\text{mol m}^{-2} \text{ s}^{-1}$ and high light (HL) at $1000 \mu\text{mol m}^{-2} \text{ s}^{-1}$.



Supplementary Figure 2. Seven week-old *S. viridis* and *Z. mays* grown under different irradiances. Low light at $100 \mu\text{mol m}^{-2} \text{s}^{-1}$ and high light at $1000 \mu\text{mol m}^{-2} \text{s}^{-1}$. (A) Low light-grown *S. viridis*, (B) high light-grown *S. viridis*, (C) low light-grown *Z. mays*, and (D) high light-grown *Z. mays*. Red arrowhead points to the leaf used for measurements and quantification. Bar = 20 cm.



Supplementary Figure 3. Dark respiration rates of *S. viridis* (A) and *Z. mays* (B) grown under different growth irradiances. Each bar represents the mean \pm SE, $n=3$. Letters indicate the ranking (lowest= a) using multiple-comparison Tukey's post-hoc test. Bars with same letter are not statistically different at $P<0.05$.